NJC

PAPER

View Article Online
View Journal | View Issue

Cite this: *New J. Chem.*, 2018, **42**, 10124

Novel nano-dyad of homoleptic sandwich-type phthalocyanines with nitrogen doped graphene quantum dots for nonlinear optics†

David O. Oluwole,* Njemuwa Nwaji, Lindokhuhle C. Nene, Lesedi Mokone, Edith Dube and Tebello Nyokong*

Received 9th April 2018,
Accepted 1st May 2018

DOI: 10.1039/c8nj01707g

rsc.li/njc

The syntheses of neodymium(III) 2,9,16,23-tetrakis-(2,6-di-*tert*-butyl-4-methylphenoxy)phthalocyanine (**2**), bis europium(III) 2,9,16,23-tetrakis-(2,6-di-*tert*-butyl-4-methylphenoxy)phthalocyanine (**3**), bis dysprosium(III) 2,9,16,23-tetrakis-(2,6-di-*tert*-butyl-4-methylphenoxy)phthalocyanine (**4**) and their conjugated analogues with nitrogen doped quantum dots (NGQDs) are reported herein. The optical nonlinearity of the sandwich-type phthalocyanine complexes and their conjugates with NGQDs were studied in dimethyl sulfoxide using the open aperture Z-scan technique at an excitation wavelength of 532 nm with a 10 ns pulse. The nonlinear absorption coefficient (β_{eff}) value of the samples ranges from 15 cm GW^{-1} to 89.6 cm GW^{-1}. Complex **4** and its conjugates afforded a strong optical limiting behaviour compared to the other samples. These fabricated complexes and their conjugates with NGQDs could serve as a plausible nonlinear optical (NLO) material due to their fascinating NLO properties.

Introduction

Sandwich-type phthalocyanines (Pcs) and graphene quantum dots (GQDs) continue to receive tremendous research focus in nonlinear optics in a bid to design and develop novel efficient nonlinear optical (NLO) materials capable of impeding a high amplitude laser beam whilst allowing the transmittance of low intensity light.[1–4] Sandwich-type Pcs are known to exhibit fascinating NLO features with a large nonlinear absorption coefficient (β_{eff}), inherent fast response time and efficient limiting threshold intensity or fluence (I_{lim}) due to their extensive π-electron conjugated ring system, strong intramolecular π–π interaction, unique electronic characteristics, and chemical and photothermal stability.[1,5–7] The use of the lanthanide atom as the central metal is known to enhance triplet state parameters which improves the overall nonlinear optical performance of sandwich-type Pcs.[1,7,8]

On the other hand, graphene quantum dots (GQDs) are zero-dimensional carbon-based materials with a unique physicochemical behaviour such as intrinsic optical activity, high electrical conductivity, excellent optical transparency, mechanical flexibility, large surface area, thermal and chemical stability.[9,10] The ultrafast carrier dynamics and large absorption of incident light per layer make graphene a fast-saturable absorber over a wide spectral range.[11] GQDs are known to exhibit strong quantum confinement and edge effects which affords them good photophysical properties.[12] GQDs when alone or in combination with other molecules have been reported to depict interesting NLO characteristics.[4,13–17] Nitrogen doped GQDs (NGQDs) are known to have distinct and enhanced physical and chemical properties compared to their pristine form (GQDs) owing to their chemically-bonded N atom which manipulates their chemical reactivity and electronic properties.[15] These unique features have afforded them applicability in different fields such as electrocatalysis[16] and nonlinear optics.[17] Additionally, NGQDs are innocuous compared to cadmium based QDs.[18,19]

In this study, nitrogen doped GQDs (NGQDs) are non-covalently interacted with sandwich-type Pcs *via* π–π stacking for the first time. Previously, mononuclear phthalocyanines have been interacted with GQDs *via* covalent linkage or π–π stacking[13] with improved NLO behaviour but to the best of our knowledge no studies have been reported on the interaction of NGQDs with sandwich-type Pcs.

Hence, we report for the first time the synthesis and NLO behaviour of bis neodymium(III) 2,9,16,23-tetrakis-(2,6-di-*tert*-butyl-4-methylphenoxy)phthalocyanine (**2**), bis europium(III) 2,9,16,23-tetrakis-(2,6-di-*tert*-butyl-4-methylphenoxy)phthalocyanine (**3**), bis dysprosium(III) 2,9,16,23-tetrakis-(2,6-di-*tert*-butyl-4-methylphenoxy)phthalocyanine (**4**) and their conjugated analogues with NGQDs. The variation in the central metal of the Pcs is

Center for Nanotechnology Innovation, Department of Chemistry, Rhodes University, Grahamstown 6140, South Africa. E-mail: t.nyokong@ru.ac.za, davido.oluwole@gmail.com; Fax: +27 46 6225109; Tel: +27 46 6038260

† Electronic supplementary information (ESI) available. See DOI: 10.1039/c8nj01707g

expected to influence the NLO behavior of these Pcs. In addition, the di-*tert*-butyl-4-methylphenoxy substituents are expected to afford good solubility in most organic solvents and give high triplet quantum yields due to the phenoxy *tert*-butyl ring substituents.[20] The combination of the sandwich-type Pcs with N-doped GQDs is expected to afford improved optical nonlinearity since they are both NLO materials. The samples will be studied in dimethyl sulfoxide by the open aperture Z-scan technique with a laser excitation wavelength of 532 nm with a 10 ns pulse.

Experimental

Materials

Neodymium(III) acetylacetonate, dysprosium(III) acetylacetonate, europium(III) acetylacetonate, 1-pentanol, 1,8-diazabicylo[5.4.0]-undec-7-ene (DBU), isoamyl alcohol, aluminium oxide 90 active neutral, *n*-octanol, and Bio-Beads S-X1 were obtained from Sigma Aldrich®. Ultra-pure water was obtained from a Milli-Q Water System (Millipore Corp., Bedford, MA, USA). Chloroform and methanol (MeOH) were procured from SAARCHEM®. All other reagents and solvents were sourced from commercial suppliers and used as received. The syntheses of 2,6-di-*tert*-butyl-4-methylphenoxy phthalonitrile[21] and nitrogen doped graphene quantum dots[22] have been reported earlier.

Equipment

Mass spectral data were acquired on a Bruker® AutoFLEX III Smartbeam TOF/TOF Mass spectrometer. The instrument was operated in the positive ion mode. The spectra were obtained using alpha-cyano-4-hydroxycinnamic acid as the MALDI matrix and a 354 nm nitrogen laser. Ground state electronic absorption was measured on a Shimadzu® UV-2550 spectrophotometer. FT-IR spectra were recorded on a Bruker® ALPHA FT-IR spectrometer with a universal attenuated total reflectance (ATR) sampling accessory.

^{1}H-NMR measurement was done using a Bruker® AVANCE II 600 MHz NMR spectrometer with tetramethylsilane (TMS) as an internal reference. X-ray powder diffraction patterns were recorded using Cu Kα radiation (1.5405 Å, nickel filter) equipped with a LynxEye detector, on a Bruker® D8 Discover equipped with a proportional counter as previously described.[23] The morphology of the NGQDs and their conjugates were assessed using a transmission electron microscope (TEM) ZEISS LIBRA® model 120 operated at 90 kV accelerating voltage. Magnetic circular dichroism (MCD) spectra were measured with a Chirascan® plus spectrodichrometer equipped with a 1 T (tesla) permanent magnet by using both the parallel and antiparallel fields.

Z-Scan measurements were performed as described in the literature using a frequency-doubled Nd:YAG laser (Quanta-Ray, 1.5 J/10 ns fwhm pulse duration) as the excitation source.[24]

Syntheses

Metal free 2,9,16,23-tetrakis-(2,6-di-*tert*-butyl-4-methylphenoxy)-phthalocyanine (1), Scheme 1A. The metal free 2,9,16,23-tetrakis-(2,6-di-*tert*-butyl-4-methylphenoxy)phthalocyanine (**1**) was synthesized as follows: 4-(2,6-di-*tert*-butyl-4-methylphenoxy)-phthalonitrile (1.00 g, 2.89 mmol) was dissolved in 1-pentanol (5 mL) and DBU (0.3 mL, 1.93 mmol) was added. The reaction mixture was refluxed at ~140 °C for 6 h in the presence of argon flow. The reaction was monitored with UV-vis and mass spectroscopy. On completion, the UV-vis spectrum of the complex depicted a split Q-band and the crude blue-green product was cooled to ambient temperature. This was followed by evaporation to dryness and subsequent purification by aluminium oxide 90 active neutral packed column chromatography with a gradient eluent mixture of methanol and $CHCl_3$.

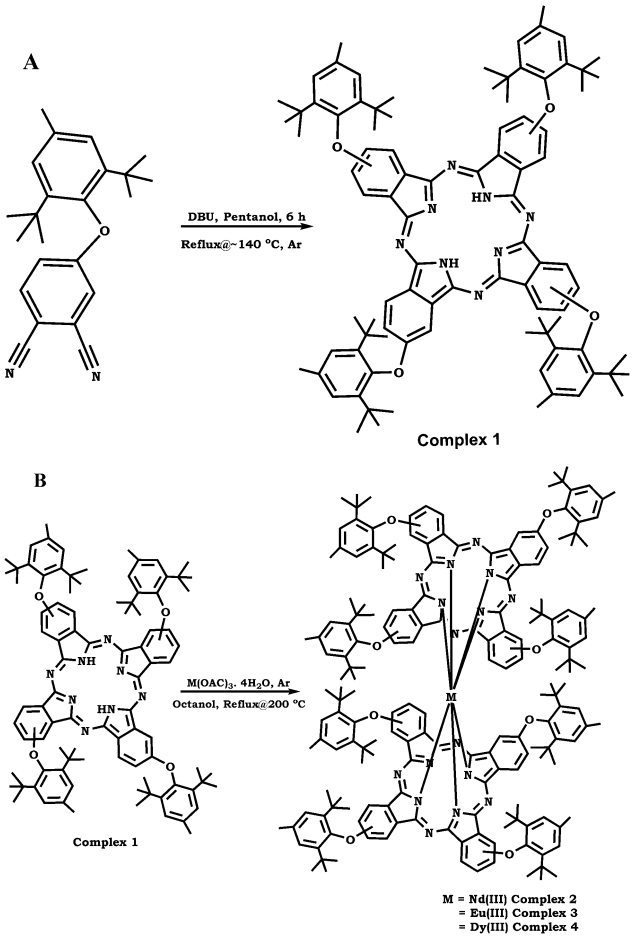

Scheme 1 Synthetic pathway for sandwich-type phthalocyanines (bis neodymium(III) 2,9,16,23-tetrakis-(2,6-di-*tert*-butyl-4-methylphenoxy)-phthalocyanine (**2**), bis europium(III) 2,9,16,23-tetrakis-(2,6-di-*tert*-butyl-4-methylphenoxy)phthalocyanine (**3**), bis dysprosium(III) 2,9,16,23-tetrakis-(2,6-di-*tert*-butyl-4-methylphenoxy)phthalocyanine (**4**)).

UV-vis ($CHCl_3$): λ_{max}/nm: 340, 601, 661, 697. Calculated for $C_{92}H_{106}N_8O_4$; (C 79.62, H 7.70, N 8.07)% found – (C 79.27, H 7.20, N 8.02)%; NMR ($CDCl_3$, 600 Hz): δ, 9.51–9.31 (12H, m, Pc macrocycle-H), 8.04–6.67 (8H, m, phenyl-H), 1.63 (12H, m, methyl-H), 1.45–1.43 (72H, m, butyl-H), 0.09 (2H, m, NH_2-H); IR [(KBr) ν_{max}/cm^{-1}]: 1650 (–C–C–), 1457 (–C–H–), 1380 (–C–N–), 1239 (–C–O–C–), 1156 (–C–O–); MS (MALDI-TOF) (*m*/*z*): calcd 1386.83 for $C_{92}H_{106}N_8O_4$; found: $[M + H]^+$ 1387.73.

Bis neodymium(III) 2,9,16,23-tetrakis-(2,6-di-*tert*-butyl-4-methylphenoxy)phthalocyanine (2), Scheme 1. Neodymium(III) acetylacetonate hydrate (0.100 g, 0.226 mmol) and complex **1** (0.150 g, 0.108 mmol) were dissolved in *n*-octanol. DBU (0.100 mL, 0.644 mmol) was added into the mixture, followed by refluxing at ~200 °C under argon flow for 12 h. The obtained sticky green product was evaporated to dryness and separated by an aluminium oxide 90 active neutral packed column with gradient eluents of hexane:$CHCl_3$. The isolated and purified product was further purified on an MnO_2/Al_2O_3 packed column with a gradient eluent mixture of MeOH in $CHCl_3$. The obtained isolate was finally purified on a Bio-Beads S-X1 packed column and air dried in an enclosed fume hood.

Yield: 0.04 g (w/w), UV-vis (DMSO): λ_{max}/nm ($\log\varepsilon$): 342 (4.78), 562 (3.74), 648 (4.86); calculated for $C_{184}H_{208}NdN_{16}O_8$; (C 75.79, H 7.19, N 7.69)% found – (C 74.36, H 8.03, N 7.63)%; NMR ($CDCl_3$, 600 Hz): δ, 8.19–7.82 (24H, m, Pc macrocycle-H), 6.93–6.56 (16H, m, phenyl-H), 1.63 (24H, m, methyl-H), 0.82–0.76 (144H, m, butyl-H); IR [(KBr) ν_{max}/cm^{-1}]: 1637 (–C–C–), 1481 (–C–H–), 1360 (–C–N–), 1309 ($Pc^{\bullet-}$), 1257 (–C–O–C–), 1204 (–C–O–); MS (MALDI-TOF) (*m*/*z*): calcd 2911.54 for $C_{184}H_{208}NdN_{16}O_8$; found: $[M - H]^-$ 2910.07.

Bis europium(III) 2,9,16,23-tetrakis-(2,6-di-*tert*-butyl-4-methylphenoxy)phthalocyanine (3), Scheme 1. Complex **3** was synthesized and purified as earlier described for complex **2** but using europium acetylacetonate instead of neodymium acetylacetonate. The reaction amounts, conditions and purification were as outlined for **2**.

Yield: 0.05 g (w/w), UV-vis (DMSO): λ_{max}/nm ($\log\varepsilon$): 343 (5.06), 541 (5.08), 643 (4.89); calculated for $C_{184}H_{208}EuN_{16}O_8$; (C 75.59, H 7.17, N 7.67)% found – (C 75.71, H 7.54, N 7.80)%; NMR ($CDCl_3$, 600 Hz): δ, 8.53–8.06 (24H, m, Pc macrocycle-H), 7.62–6.57 (16H, m, phenyl-H), 1.89–1.70 (24H, m, methyl-H), 1.70–1.64 (144H, m, butyl-H); IR [(KBr) ν_{max}/cm^{-1}]: 1627 (–C–C–), 1451 (–C–H–), 1365 (–C–N–), 1319 ($Pc^{\bullet-}$), 1249 (–C–O–C–), 1201 (–C–O–); MS (MALDI-TOF) (*m*/*z*): calcd 2922.56 for $C_{184}H_{208}EuN_{16}O_8$; found: $[M + 3H]^+$ 2925.02.

Bis dysprosium(III) 2,9,16,23-tetrakis-(2,6-di-*tert*-butyl-4-methylphenoxy)phthalocyanine (4), Scheme 1. Complex **4** was synthesized and purified as earlier described for complex **2**, but using dysprosium acetylacetonate instead of neodymium acetylacetonate. The reaction amounts, conditions and purification were as outlined for **2**.

Yield: 0.04 g (w/w), UV-vis (DMSO): λ_{max}/nm ($\log\varepsilon$): 342 (4.78), 562 (3.74), 648 (4.86); calculated for $C_{184}H_{208}DyN_{16}O_8$; (C 75.32, H 7.15, N 7.64)% found – (C 75.64, H 8.14, N 7.63)%; NMR ($CDCl_3$, 600 Hz): δ, 8.19–7.82 (24H, m, Pc macrocycle-H), 6.92–6.49 (16H, m, phenyl-H), 1.15–1.07 (24H, m, methyl-H), 0.82–0.76 (144H, m, butyl-H); IR [(KBr) ν_{max}/cm^{-1}]: 1649 (–C–C–), 1457 (–C–H–), 1361 (–C–N–), 1314 ($Pc^{\bullet-}$), 1246 (–C–O–C–), 1202 (–C–O–); MS (MALDI-TOF) (*m*/*z*): calcd 2933.57 for $C_{184}H_{208}DyN_{16}O_8$; found: $[M + 3H]^+$ 2936.98.

Interaction of N-doped graphene quantum dots (NGQDs) with complexes 2 to 4, Scheme 2. The non-covalent interaction of the NGQDs and the Pc complexes was achieved as follows: 10 mg mL^{-1} each of complexes **2** to **4** in tetrahydrofuran (THF) were separately measured into flasks containing 15 mg mL^{-1} NGQDs in ultra-pure water. The mixture was sonicated in an ultrasonic bath for 4 h to foster the effective interaction of the NGQDs and the complexes (**2** to **4**). The resultant solution was further stirred at ambient temperature for 72 h leading to the formation of NGQDs and sandwich-type Pcs conjugates. The formed conjugates were isolated and successively purified with methanol under centrifugation and dried in an enclosed fumehood. The obtained conjugates are denoted as: **2**–NGQDs, **3**–NGQDs and **4**–NGQDs.

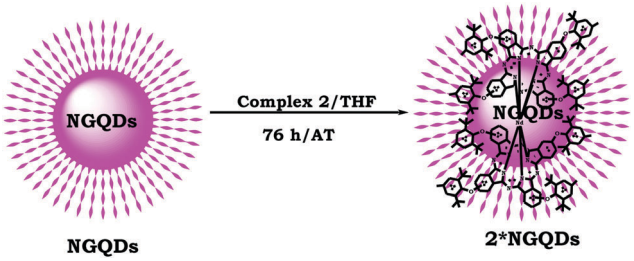

Scheme 2 Representative synthetic pathway for π–π stacking of sandwich-type phthalocyanines with NGQDs using complex **2** as an example. AT = ambient temperature and THF = tetrahydrofuran.

Z-Scan measurements

The nonlinear optical parameters for the sandwich-type Pcs and their conjugates with NGQDs were obtained by the open aperture Z-scan technique using eqn (1)[25,26]

$$T(z) = \frac{1}{\sqrt{\pi}q_0(z)}\int_{-\infty}^{\infty} \ln\left[1 + q_0(z)e^{\tau^2}\right]d\tau \quad (1)$$

where $q_0(z)$ is an indicator showing the strength of the nonlinearity. For a circular Gaussian beam, $q_0(z)$ is given by eqn (2).

$$q_0(z) = \frac{2\beta P_0 l_{eff}}{\pi\omega_0(z)^2} \quad (2)$$

where β is the effective nonlinear absorption coefficient of the material, P_0 is the peak power of the pulses, z is the sample position and l_{eff} is the effective path length, given by eqn (3):

$$l_{eff} = \frac{1 - e^{-\alpha l}}{\alpha} \quad (3)$$

where α and l are the linear absorption coefficient and path-length, respectively.

The least square regression method was used to fit all the Z-scan data with eqn (1) and (2). The effective absorption coefficient β_{eff} and the beam waist ω_0 were treated as free parameters in the fit. For a given sample, the beam waist is altered by intensity, hence treating the beam waist and effective nonlinear absorption coefficient as free parameters is an acceptable method in the literature.[27]

Results and discussion

Characterization of sandwich-type Pcs alone

An analogous template synthetic pathway was applied for the formation of the sandwich-type Pcs. Metal free 2,9,16,23-tetrakis-(2,6-di-*tert*-butyl-4-methylphenoxy)phthalocyanine (complex **1**) was reacted with the corresponding metal acetylacetonate salts (M = Nd (**2**), Eu (**3**), Dy (**4**)) in refluxing *n*-octanol in the presence of DBU and an argon atmosphere to obtain complexes **2** to **4**, Scheme 1. The reaction progress was monitored with UV-vis and mass spectroscopies.

On completion, the formation of the complexes was confirmed by FTIR, ^{1}H NMR, MALDI-TOF mass spectroscopies and the purity was determined by elemental analyses and ^{1}H NMR. The obtained data were consistent with the predicted structures with good solubility in most organic solvents. The reduced blue forms ($[Pc(-2)Ln^{III}Pc(-2)]^-$) of the double decker (DD) complexes were predominantly obtained in the crude solution after reaction completion, as judged by the spectra. The Q band of the green neutral form ($Pc(-2)Ln^{III}Pc(-1)$) is red-shifted compared to that of the blue form.[28] The latter typically has a shoulder near 700 nm, resulting in a Q band that appears split, as observed in this work during synthesis and purification using alumina packed column chromatography. To obtain the target neutral green forms of the DD complexes, a column containing alumina coated with MnO_2 (MnO_2/Al_2O_3) was employed as previously described.[29] In this way, the target oxidized DD complexes were obtained in qualitative yields.

The ^{1}H NMR spectra of complex **1** depicted a multiplet resonating at 9.51–9.31 ppm affording 24 protons on integration corresponding to the Pc aromatic protons while the phenyl ring showed a multiplet resonating at 8.04–6.67 ppm with 8 protons and the methyl substituents depicted multiplets accounting for 12 protons with a resonance signal at 1.63 ppm. The butyl substituents showed multiplets with a resonance signal at 1.45–1.43 ppm affording 72 protons on integration and the 2 inner protons resonating at 0.09 ppm. Complex **2** depicted a multiplet resonating at 8.19–7.82 ppm and gave 24 protons on integration which correspond to Pc aromatic protons while the phenyl ring showed a multiplet resonating at 6.93–6.56 ppm with 16 protons and the methyl substituents depicted multiplets accounting for 24 protons with a resonance signal at 1.63 ppm. The butyl substituents showed multiplets with a resonance signal at 0.82–0.72 ppm affording 144 protons on integration. Complexes **3** and **4** showed a similar trend to **2** with relative chemical shifts in the resonance signals, see Experimental section.

The obtained mass spectra data of the complexes were in accordance with the proposed mass to charge ratio as revealed by the MS spectra (Fig. S1, ESI†). The FT-IR benchmark vibrational bands for the DD complexes were observed at 1309 cm^{-1}, 1319 cm^{-1} and 1314 cm^{-1} for complexes **2** to **4**, respectively (Fig. 1). The appearance of the structural IR benchmark for the DDs due to the monoanion radical ($Pc^{\bullet -}$), Fig. 1, confirms the formation of the green form ($Pc(-2)Ln^{III}Pc(-1)$).

The ground state electronic absorption in DMSO (Fig. 2A) and MCD spectra for complexes **2** to **4** in chloroform showed

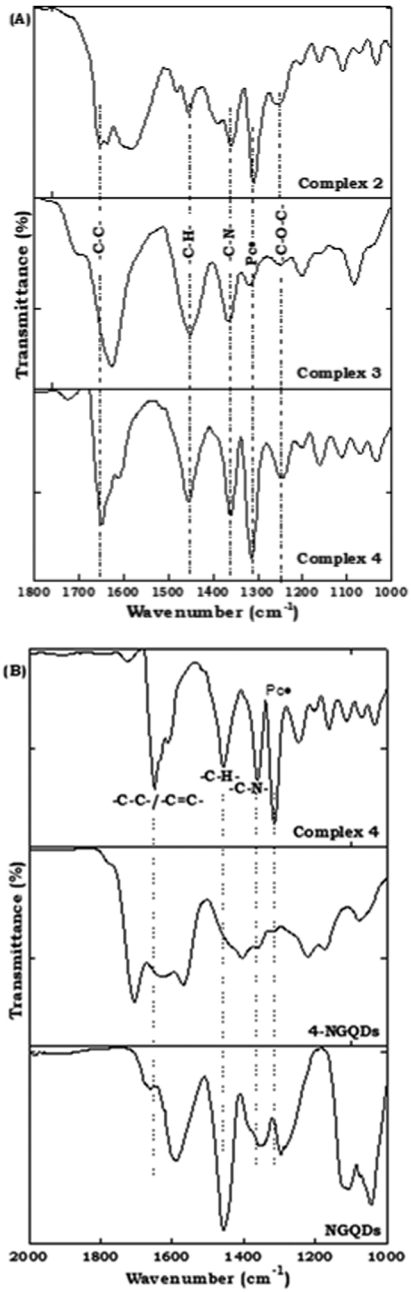

Fig. 1 FT-IR spectra for complexes **2** to **4** (A) and their conjugates with GQDs (B) showing the disappearance of the double decker Pc IR benchmark mark.

bands typical of double decker (DD) complexes, Fig. 2. In DMSO, the spectra (Fig. S2A, ESI†) was typical of the blue form ($[Pc(-2)Ln^{III}Pc(-2)]^-$) with a split Q band.[28] Thus, DMSO reduces the green form to the blue form. Studies done in DMSO will be those of the latter. The Q band position of the DD complexes is dependent on the size of the lanthanide metal inferring the effect of central metal on the Pcs. The metal free ligand (complex **1**) afforded the split Q-band (Fig. 2A) which is typical of unmetalated Pcs but on metalation with the corresponding lanthanide acetylacetonate salt (M = Nd (**2**), Eu (**3**), Dy (**4**)), the split Q-band vanished with the appearance of a

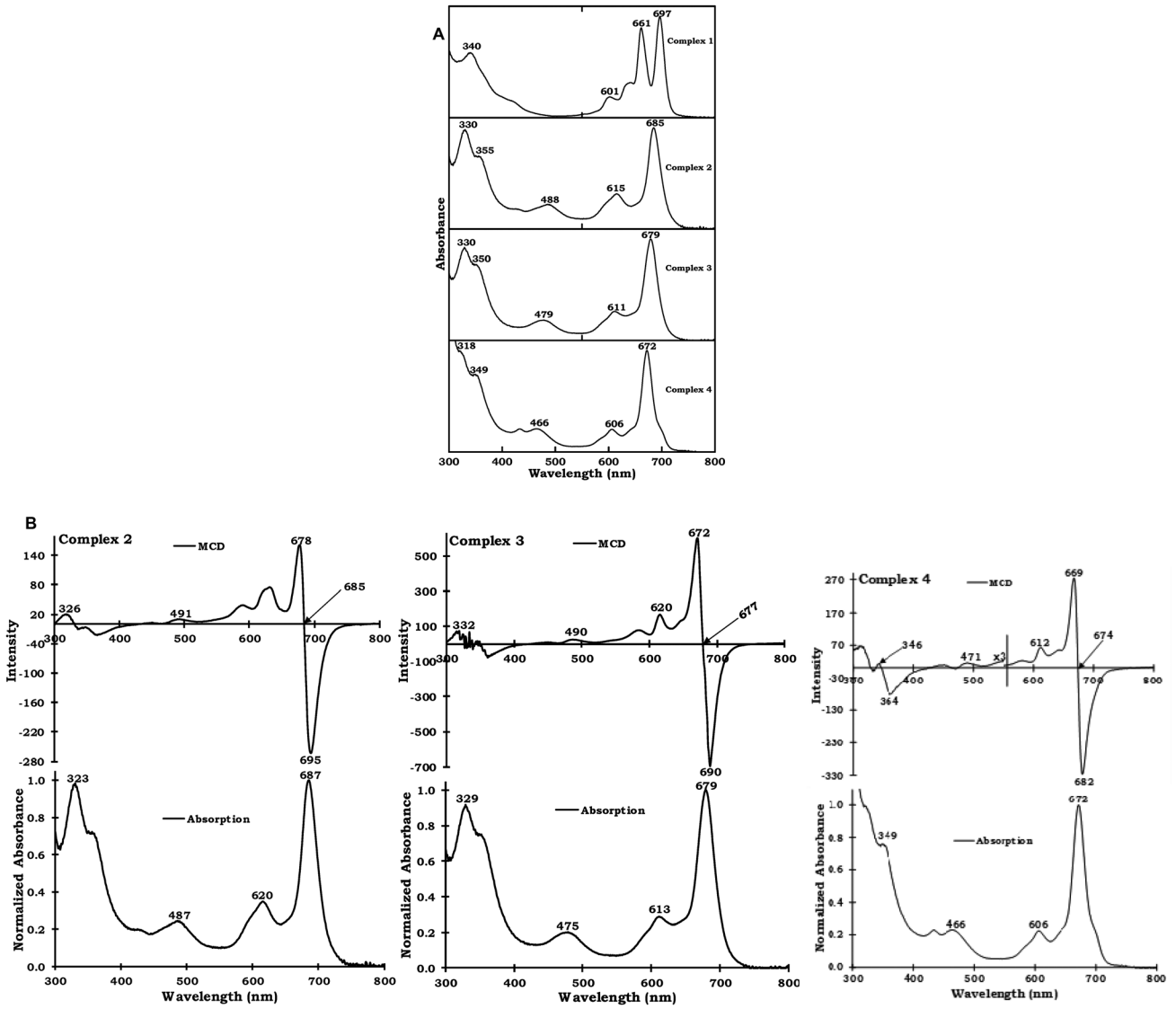

Fig. 2 (A) Ground state electronic absorption spectra for complexes **2** to **4** in chloroform and (B) MCD and ground state electronic absorption spectra for complexes **2** to **4** in chloroform.

monomeric Q-band which is typical of metalated Pcs. In addition, there is the emergence of the blue valence band (π-radical band) at 488 nm, 479 nm, 466 nm for complexes **2** to **4**, respectively, (Fig. 2A). The presence of the π-radical band evidenced by UV-vis for complexes **2** to **4** in chloroform supports the observed Pc structural IR benchmark observed at 1309 cm^{-1}, 1319 cm^{-1} and 1314 cm^{-1} for complexes **2** to **4**, respectively. The UV-vis spectra of complexes **2** to **4** were measured at concentrations ranging from 2.90×10^{-6} to 1.35×10^{-5} mol in DMSO, Fig. S2B (ESI†). The Beer–Lambert law was obeyed at the studied gradient concentrations.

MCD spectroscopy can be used to obtain vital information about band polarizations, ground and excited state degeneracies that cannot be exclusively obtained using UV-vis absorption spectra only.

Accurate analysis of the Faraday terms, A_1, B_0 and C_0 forms the basic theory of MCD spectroscopy and these terms depend upon the Zeeman splitting of the degenerate excited states, the field induced mixing of states and the Zeeman splitting of degenerate ground states,[30] respectively. Fig. 2B shows the absorption and corresponding MCD spectra of complexes **2** to **4** in chloroform. A sigmoid curve splitting with the Faraday A_1 term was observed between 600 nm and 700 nm region on the MCD spectra of **2** to **4** with cross-over points at 685 nm, 677 nm and 674 nm, respectively. which essentially correspond to the Q band absorption maxima of the complexes, suggesting that the main ππ* excited state retains its orbital degeneracy. A similar observation was also recorded between the 300 nm and 400 nm region with cross-over points at 325 nm, 332 nm and 346 nm for **2** to **4**, respectively also indicating the excited state degeneracy in this region.

The changes in the spectra of sandwich-type phthalocyanines can be interpreted based on excitonic (EC) states due to the excitation of a single Pc ring as well as the charge

resonance (CR) states generated by charge transfer between Pc rings.[31] Generally, a lower-energy band with lower intensity mainly arises from a transition with a more CR character and a more intense band at a slightly higher energy arises primarily from an EC interaction. Thus, the bands observed at 687 nm, 679 nm and 672 nm in the UV-vis spectra for **2** to **4** can be assigned to the Q band arising from EC- and CR-dominated transitions. The observed Faraday *B*-terms band at 491 nm, 490 nm and 471 nm in MCD spectra of complexes **2** to **4** are essentially a superimposition of the 487 nm, 475 nm and 466 nm observed in the corresponding UV absorption spectra, indicating the non-degeneracy of this region.

Characterization of the NGQDs and their conjugated analogs with sandwich-type Pcs

Scheme 2 depicts a representative pathway for the formation of the nanocomposites of NGQDs and complexes *via* π–π stacking.

FT-IR spectra

The Fourier transform infrared was used to access the possible interaction between the NGQDs and the complexes. The spectra of all the complexes exhibited all the expected vibrational bands with the clear observation of the DD Pc structural IR benchmark (Fig. 1A) while a disappearance of the Pc structural IR benchmark was seen in the conjugates which is evidenced by the FT-IR spectra (Fig. 1B and Fig. S3, ESI†). The UV-vis spectra of the conjugates further corroborates the disappearance of the Pc structural IR benchmark, Fig. S4 (ESI†) (using NGQDs and complex **2** as an example).

Morphology determination

The NGQDs depicted a broad diffraction pattern inferring the amorphous nature of the particles and this is evidenced by the XRD diffractogram (Fig. 3). The Pcs depicted a broad diffraction pattern at $2\theta = 25^{\circ}$ which is typical of phthalocyanines.[32] The NGQDs also shows a typical broad peak.[13]

Following conjugation, there are some sharp peaks most likely due to the increase in size. The TEM micrograph exhibited polydisperse spherical particles which is typical of graphene quantum dots. The TEM micrograph of the conjugate showed an aggregated particle which might be attributed to plausible π–π stacking (Fig. 4). The average size diameter for the NGQDs was found to be 3.8 nm (Fig. S5, ESI†) but their sizes could not be obtained on conjugation with Pcs due to the aggregation earlier stated.

UV-vis absorption

The ground state absorption spectra of the conjugates showed the disappearance of the Pc structural IR benchmark, Fig. S4 (ESI†) (using NGQDs and complex **2** as an example).

Nonlinear optical studies

Fig. 5 shows the open aperture Z-scan signatures for the complexes and their conjugates with NGQDs.

The reverse saturable absorption mechanism for phthalocyanine can be described by the general five level model,

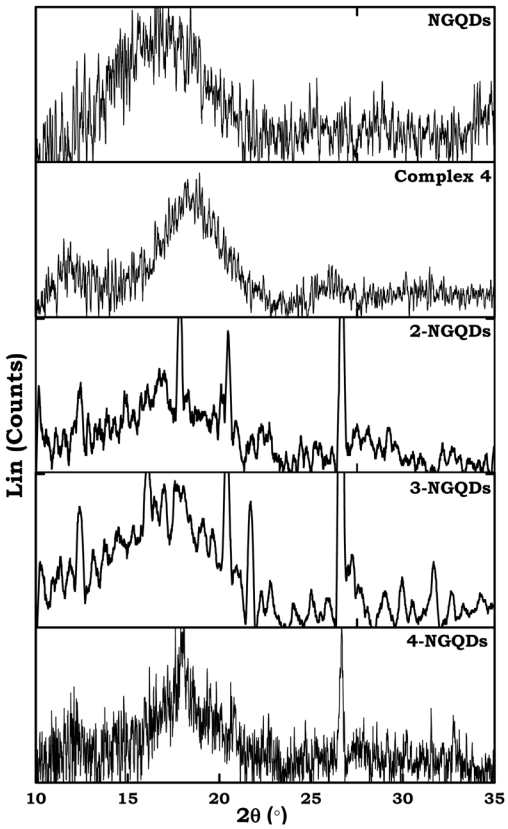

Fig. 3 XRD diffractograms for complex **4**, NGQDs and their conjugates with Pcs.

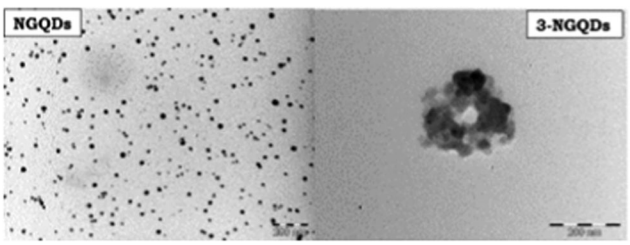

Fig. 4 TEM micrographs for NGQDs and their conjugates with Pcs using **3**–NGQDs as an example. Magnification = 200 nm.

Fig. 6.[27,33] In this model, initial excitation of the ground state (S_0) led to either the population of the first excited singlet (S_1) or the higher excited singlet (S_2) with the excited state absorption cross-section δ_1. Rapid relaxation of electrons from S_2 to S_1 occurs due to the short lifetime of S_2 resulting in population of the excited triplet through intersystem crossing with the time constant (τ_{isc}). Further absorption of the laser radiation excites molecules from the first excited triplet (T_1) state to the higher excited triplet (T_2) state with the absorption cross-section δ_2. Rapid relaxation from T_2 to T_1 occurs similar to S_2.

When a laser with a nanosecond pulse duration is employed as is the case in this work, the pulse duration is far longer than the upper excited singlet or triplet, hence these states can be ignored.[34] Thus, the rate equations needed

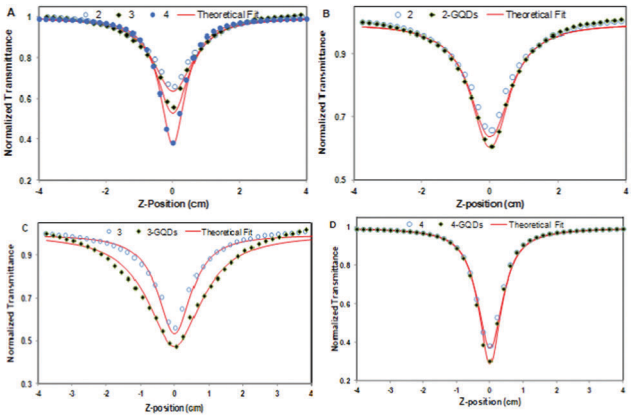

Fig. 5 Comparative open aperture Z-scan curves for complexes **2** to **4** and their conjugates with NGQDs in DMSO. α = 0.5 cm^{-2}, excitation at 532 nm with a 10 ns laser pulse rate. Normalized transmission plotted as a function of sample position on the *Z*-axis.

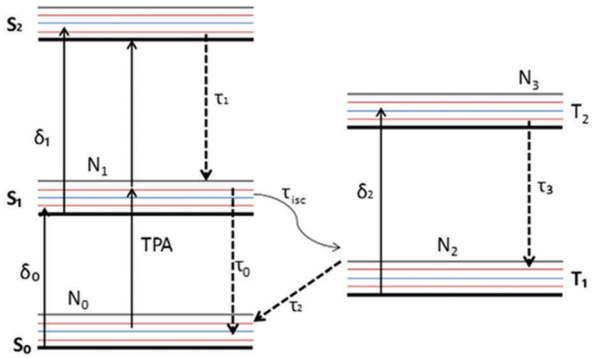

Fig. 6 Five level energy diagram explaining the dynamics of the excited state population (upward arrows), non-radiative relaxation (dashed arrows) in the studied complexes.

to describe the five level models now reduces to three differential rate eqn (4)–(6).

$$\frac{\partial N_0}{\partial t} = -\frac{\delta_0 I}{h\nu}N_0 + \frac{N_1}{\tau_0} + \frac{N_2}{\tau_2} \quad (4)$$

$$\frac{\partial N_1}{\partial t} = \frac{\delta_0 I}{h\nu}N_0 - \frac{N_1}{\tau_{isc}} - \frac{N_1}{\tau_0} \quad (5)$$

$$\frac{\partial N_2}{\partial t} = -\frac{N_1}{\tau_{isc}} - \frac{N_2}{\tau_2} \quad (6)$$

where N_0, N_1 and N_2 are the populations of S_0, S_1, and T_1 respectively, δ_0 is the ground state absorption cross-section, h is Planck's constant, ν is optical frequency and τ_{isc} is the intersystem crossing lifetime, and the τ_i values are the lifetimes of the excited states. The attenuation of laser beam radiation is governed by a propagation eqn (7), where the excited state absorption from S_1 and T_1 are included in the absorption coefficient.

$$\frac{\partial I}{\partial z} = -\alpha(I) = -(\delta_0 N_0 + \delta_1 N_1 + \delta_2 N_2)I \quad (7)$$

where δ_1 and δ_2 are the absorption cross-sections of the singlet and triplet state respectively.

The steady state approximation under this case, becomes a valid approach for solving the above equations.[27,35] The equations can be analytically solved and the intensity dependent absorption coefficient becomes eqn (8).

$$\alpha(I) = \frac{\sigma_0 N}{1 + \frac{I}{I_{sat}}}\left[1 + \frac{\sigma_1}{\sigma_2}.\frac{\tau_{isc}}{\tau_2}.\frac{I}{I_{sat}} + \frac{\sigma_2}{\sigma_0}.\frac{I}{I_{sat}}\right] \quad (8)$$

where $\alpha_0 = \sigma_0 N$ is the ground state linear absorption coefficient (N is the total number density of the dissolved molecules). $I_{sat} = \frac{h\nu}{(\sigma_0 \tau_0)}$ is the intensity of saturation and k is the ratio of the excited state to ground state cross-sections.

In phthalocyanines and other related macrocycles, σ_2 and σ_1 re approximately the same order when $\tau_{isc} \ll \tau_2$. Thus, the term with σ_1 on the numerator can be eliminated and the intensity dependent absorption coefficient can be now defined as eqn (9):

$$\alpha(I, I_{sat} \cdot k) = \frac{\alpha_0}{1 + \frac{I}{I_{sat}}}\left(1 + k\frac{I}{I_{sat}}\right) \quad (9)$$

Since the absorption of the excited state is predominantly from the triplet state, then the ratio of the excited to ground state absorption cross-section (k) is expressed as $\frac{\sigma_2}{\sigma_0}$. The parameter I/I_{sat} in the equation can be replaced with F/F_{sat}, where F and F_{sat} are the fluence per pulse and the energy density of saturation defined as the energy density at which the output reaches saturation value. A prerequisite requirement for good optical limiting material is possession of high k, low F_{sat}, low α_0 and high β_{eff} values.[27,35] The optical limiting parameters k and F_{sat} were obtained by substituting $\alpha(I,I_{sat}{\cdot}k)$ back to the propagation formalism eqn (7) prior to fitting the open aperture data. Integration over a homogenous sample of thickness L yield a transcendental eqn (10) for transmission T as $T = I_{out}/I_{in}$.[33]

$$T(F, k, F_{sat}) = \exp^{(-\alpha_0 L)} \times \left(\frac{F_{sat} + kT(F \cdot k \cdot F_{sat})F}{F_{sat} + KF}\right)^{1-\frac{1}{k}} \quad (10)$$

The normalized transmittance was numerically evaluated and plotted against incident energy density per pulse (J cm^{-2}) (Fig. 7A and B) for investigation of the optical limiting properties with k and F_{sat} being treated as free parameters in the fitting algorithm. A comprehensive literature review of 40 optical limiting materials by O'Flaherty *et al.* showed the value of F_{sat} within the range of 5–150 J cm^{-2}, β_{eff}: 10^{-9}–10^{-8} cm W^{-1} and k: 2–27 in solution.[27]

The obtained values of β_{eff}, F_{sat} and k for the complexes and the nanoconjugates in this work are shown in Table 1.

In DMSO, these values are for the blue form, which is known to show improved NLO behaviour. The observed values of β_{eff}, F_{sat} and k for the complexes alone as well as the conjugates in this work are in agreement with those reported in the literature[7,33,36–38] (Table S1, ESI†). The β_{eff} values for the

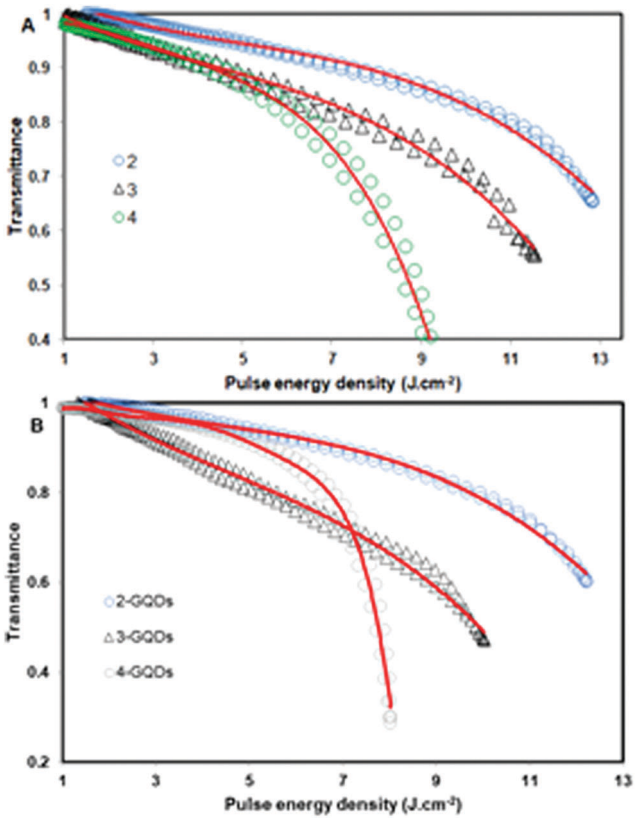

Fig. 7 Plot of normalized transmission against pulse energy density for complexes **2** to **4** (A) and their conjugates with NGQDs (B). Solid lines are theoretical fit curves.

conjugates of complexes **3** and **4** are higher than those reported in the literature,[7,33,36–41] suggesting that this material possess superior optical limiting properties. **2**–NGQDs, **3**–NGQDs and **4**–NGQDs showed higher β_{eff} and saturate at an energy density lower than the corresponding complexes indicating that the incorporation of Pcs with nanoparticles could be potential means of tuning the nonlinear optical response of NLO materials. Though the complexes reported in this work showed a lower β_{eff} than those reported by Unnikrishnan *et al.*[37] for similar sandwiched Pcs, the conjugates showed higher β_{eff} or the same order of magnitude. Additionally, we observed a lower β_{eff} for the Pc and NGDs conjugates synthesised in this work compared to those reported in the literature which were covalently linked.[13] The observed variation for the conjugates could be attributed to the nature of the bonding.

In phthalocyanines, the mechanism of reverse saturable absorption (RSA) can occur only if molecules in excited state possess a higher absorption cross-section than those in the ground state,[6] hence a k value of greater than one is a prerequisite for the occurrence of (RSA). Worthy of note is the fact that the ratio of the excited state to ground state absorption cross-section k is largely dependent on the linear absorption coefficient. Thus, the linear absorption coefficient was kept constant in this study.

It was observed that the conjugates showed a higher k value than the DD complexes alone, which could be attributed to an increase in the conjugated system resulting from π–π stacking of the complexes within the NGQD framework. Additionally, the k (as well as β_{eff}) values of the samples increased with decrease in the ionic radii of the lanthanide metal ion in the center of the Pc complexes. The increase in the k value also corresponds with the increase in the RSA, which could be attributed to population of the triplet through the heavy atom effect since the linear absorption was kept constant.

An important indication of a good nonlinear optical material is the measure of the imaginary component of the third-order nonlinear susceptibility ($\mathrm{Im}[\chi^3]$) because this gives a measure of the speed of the response of an optical material to the perturbation initiated by an intense laser beam.[6] The third-order nonlinear susceptibility can be determined using eqn (11)

$$\mathrm{Im}\left[\chi^3\right] = \frac{n^2 \varepsilon_0 c \lambda \beta_{eff}}{2\pi} \quad (11)$$

where n and c are the linear refractive index (n = 1.479 for DMSO), and the speed of light respectively, ε_0 is the permittivity of free space and λ is the wavelength of the laser.

When molecules are exposed to intense laser radiation, the permanent dipole of the molecule interacts with the light which causes a bias in the average orientation of the molecule, resulting in induced hyperpolarizability. The polarizability experienced by a molecule when it is exposed to light is known as hyperpolarizability (γ) and is related to the third order susceptibility eqn (12)

$$\gamma = \frac{\mathrm{Im}[\chi(3)]}{f^4 C_{mol} N_A} \quad (12)$$

where C_{mol} is the molar concentration of the active species in the triplet state, f is the Lorentz local field enhancement factor defined as $f = (n^2 + 2)/3$; n is the refractive index of the sample and N_A is the Avogadro constant.

Table 1 Optical limiting parameters for complexes **2** to **4** and their conjugates with NGQDs at the linear absorption coefficient (α_0) = 0.5 cm^{-1}. Solvent = DMSO

Samples	β_{eff} (cm GW^{-1})	$I_m[\chi^3]$ (esu)	γ (esu)	F_{sat} (J cm^{-2})	K (δ_{ex}/δ_0)
Complex **1**	15.0	3.50×10^{-8}	3.78×10^{-27}	12.82	2.3
Complex **2**	46.0	1.07×10^{-7}	1.16×10^{-26}	10.96	3.5
Complex **3**	58.0	1.35×10^{-7}	1.46×10^{-26}	9.22	4.1
1–NGQDs	84.0	1.96×10^{-7}	2.12×10^{-26}	12.21	6.8
2–NGQDs	87.9	1.45×10^{-7}	1.63×10^{-26}	10.03	24.1
3–NGQDs	89.6	2.09×10^{-7}	2.37×10^{-26}	8.05	35.4
NGQDs	4.63	1.08×10^{-8}	1.17×10^{-27}	15.92	—

The observed (Im[χ^3]) in this work were in order of 10^{-9}–10^{-7} esu while the second order hyperpolarizability values were in the order of 10^{-28}–10^{-26} esu. Since the (Im[χ^3]) has a direct relationship with β_{eff}, complexes with higher β_{eff} also displayed higher (Im[χ^3]), Table 1. The nanoconjugates showed enhanced (Im[χ^3]) as well as (γ) values and better optical limiting response compared to the complexes alone.

The reported optimal range of hyperpolarizability values is 10^{-34} to 10^{-29} esu for Pcs in solution[42] while comprehensive literature reports[7,43] showed (Im[χ^3]) values ranging from 10^{-8}–10^{-7} esu for Pcs in solution. The observed values of (Im[χ^3]) and (γ) in this work are slightly higher than those reported in the literature, suggesting the superior optical properties of these molecules. The NLO behaviour of the complexes and the NGQDs were lower compared to the conjugates with the latter giving less efficient NLO properties but on conjugation, we observed a synergistic effect in the NLO behaviour of the Pcs and NGQDs when combined compared to their individual forms. It is important to note that β_{eff} values of the complexes alone range from 15 cm GW^{-1} to 58 cm GW^{-1} indicating a 4 times increase from complex **2** to **4** but this was not the trend for the conjugates. The lower β_{eff} for **3**–NGQDs than the **2**–NGQDs even though **3** alone showed an enhanced β_{eff} compared to **2** could be due to the loading of a higher number of **2** onto the NGQDs. Enhancement in the NLO response with increase in the number of Pcs attached to the nanoparticles has been previously reported.[44] The photophysical properties of QDs are often influenced by the size variation due to change in quantum confinement[21] but we cannot conclusively adjudge that the size of the NGQDs played an indispensable role in the overall NLO performance of the MPcs and NGQDs conjugates due to the consideration of single size of NGQD in this work.

Conclusions

The syntheses and nonlinear optical behaviour of three novel double decker sandwich-type Pcs and their conjugates with nitrogen doped graphene dots (NGQDs) were reported in this work. Complex **4** and its conjugate with NGQDs afforded the most efficient NLO property while complex **2** and its conjugate with NGQDs gave the least NLO activity. The ionic radii of the coordinating atoms of the complexes played an indispensable role in the photophysical behaviour and optical nonlinearity of the sandwich-type Pc complexes. We observed a synergistic effect in the NLO behaviour of the Pcs and NGQDs when combined compared to their individual forms. The newly developed molecules could be explored as viable NLO materials.

Conflicts of interest

There are no conflicts to declare.

Acknowledgements

This work was supported by the Department of Science and Technology (DST) Innovation and the National Research Foundation (NRF), South Africa through the DST/NRF South African Research Chairs Initiative for Professor of Medicinal Chemistry and Nanotechnology (UID 62620) as well as Rhodes University.

References

1 N. Sheng, Z. Yuan, J. Wang, W. Chen, J. Sun and Y. Bian, *Dyes Pigm.*, 2012, **95**, 627–631.
2 D. O. Oluwole, A. V. Yagodin, N. C. Mhkize, K. E. Sekhosana, A. G. Martynov, Y. G. Gorbunova, A.-Y. Tsivadze and T. Nyokong, *Chem. – Eur. J.*, 2017, **23**, 2820–2830.
3 R. Liu, J. Hu, S. Zhu, J. Lu and H. Zhu, *ACS Appl. Mater. Interfaces*, 2017, **38**, 33029–33040.
4 J. Zhu, Y. Li, Y. Chen, J. Wang, B. Zhang, J. Zhang and W. J. Blau, *Carbon*, 2011, **49**, 1900–1905.
5 L. De Boni, S. D. Corrêa and C. R. Mendonça, in *Advances in Lasers and Electro Optics*, ed. N. Costa and A. Cartaxo, INTECH, Croatia, 2010, vol. 2, pp. 34–58.
6 R. L. Sutherland, *Handbook of Nonlinear Optics*, Marcel Dekker, New York, NY, 2nd edn, 2003.
7 X. Wang, C. L. Liu, Q. H. Gong, Y. Y. Huang and C. H. Huang, *Opt. Commun.*, 2001, **197**, 83–87.
8 D. O. Oluwole and T. Nyokong, *Dyes Pigm.*, 2018, **151**, 254–262.
9 S. J. Park and S. R. Ruoff, *Nat. Nanotechnol.*, 2009, **4**, 217–224.
10 Q. Liu, B. Guo, Z. Rao, B. Zhang and J. R. Gong, *Nano Lett.*, 2013, **13**, 2436–2441.
11 Z. Sun, T. Hasan, F. Torrisi, D. Popa, G. Privitera, F. Wang, F. Bonaccorso, D. M. Basko and A. C. Ferrari, *ACS Nano*, 2010, **4**, 803–810.
12 L. A. Ponomarenko, F. Schedin, M. I. Katsnelson, R. Yang, E. W. Hill, K. S. Novoselov and A. K. Geim, *Science*, 2008, **320**, 356–358.
13 O. M. Bankole, O. J. Achadu and T. Nyokong, *J. Fluoresc.*, 2017, **27**, 755–766.
14 S. R. Sharma, K. C. Yamijala, M. Mukhopadhyay and S. K. Pati, *J. Phys. Chem. C*, 2015, **119**, 12079–12087.
15 D. Wei, Y. Liu, Y. Wang, H. Zhang, L. Huang and G. Yu, *Nano Lett.*, 2009, **9**, 1752–1758.
16 Z. Luo, S. Lim, Z. Tian, J. Shang, L. Lai, B. MacDonald, C. Fu, Z. Shen, T. Yu and J. Lin, *J. Mater. Chem.*, 2011, **21**, 8038–8044.
17 B. Anand, R. Podila, A. M. Rao, R. Philip and S. S. S. Sai, *AIP Conf. Proc.*, 2013, **1536**, 735–736.
18 Y. Zhao, Q. Liu, S. Shakoor, J. R. Gong and D. Wang, *Toxicol. Res.*, 2015, **4**, 270–280.
19 J. Sun, Q. Xin, Y. Yang, H. Shah, H. Cao, Y. Qi, J. R. Gong and J. Li, *Chem. Commun.*, 2018, **54**, 715–718.
20 J. Chen, Q. Gan, S. Y. Li, F. B. Gong, Q. Wang, Z. P. Yang, S. Q. Wang, H. J. Xu, J. S. Ma and G. Q. Yang, *J. Photochem. Photobiol., A*, 2009, **207**, 58–65.
21 G. C. Eastmond, P. C. B. Page, J. Paprotny, R. E. Richards and R. Shaunak, *Polymer*, 1994, **35**, 4215–4227.

22 D. Qu, M. Zheng, P. Du, Y. Zhou, L. Zhang, D. Li, H. Tan, Z. Zhao, Z. Xie and Z. Sun, *Nanoscale*, 2013, **5**, 12272–12277.
23 D. O. Oluwole, J. Britton, P. Mashazi and T. Nyokong, *Synth. Met.*, 2015, **205**, 212–221.
24 D. O. Oluwole, S. M. Ngxeke, J. Britton and T. Nyokong, *J. Photochem. Photobiol., A*, 2017, **347**, 146–159.
25 M. Sheik-Bahae, A. A. Said, T.-H. Wei, D. J. Hagan and E. W. Van Stryland, *IEEE J. Quantum Electron.*, 1990, **26**, 760–769.
26 G. Tsigaridas, I. Polyzos, P. Persephonis and V. A. Giannetas, *Opt. Commun.*, 2006, **266**, 284–289.
27 S. M. O'Flaherty, S. V. Hold, M. J. Cook, T. Torres, Y. Chen, M. Hanack and W. J. Blau, *Adv. Mater.*, 2003, **15**, 20–32.
28 K. E. Sekhosana and T. Nyokong, *Inorg. Chim. Acta*, 2016, **450**, 87–91.
29 A. G. Martynov and Y. G. Gorbunova, *Inorg. Chim. Acta*, 2007, **360**, 122–130.
30 J. Mack, M. J. Stillman and N. Kobayashi, *Coord. Chem. Rev.*, 2007, **251**, 429–453.
31 N. Ishikawa, *J. Porphyrins phthalocyanines*, 2001, **5**, 87–101.
32 A. W. Snow, J. R. Griffith and N. P. Marullo, *Macromolecules*, 1984, **17**, 1614–1624.
33 S. M. O'Flaherty, J. J. Doyle and W. J. Blau, *J. Phys. Chem. B*, 2004, **108**, 17313–17319.
34 F. Li, P. Lu, H. Long, G. Yang, Y. Li and Q. Zheng, *Opt. Express*, 2008, **16**, 14571–14581.
35 J. S. Shirk, R. G. S. Pong, S. R. Flom, H. Heckmann and M. Hanack, *J. Phys. Chem. A*, 2000, **104**, 1438–1449.
36 A. Santhi, V. V. Namboodiri, P. Radhakrishnan and V. P. N. Nampoori, *J. Appl. Phys.*, 2006, **100**, 053109.
37 K. P. Unnikrishnan, J. Thomas, B. Paul, A. Kurian, P. Gopinath, V. P. N. Nampoori and C. P. G. Vallabhan, *J. Nonlinear Opt. Phys. Mater.*, 2001, **10**, 113.
38 K. P. Unnikrishnan, J. Thomas, V. P. N. Nampoori and C. P. G. Vallabhan, *Appl. Phys. B: Lasers Opt.*, 2002, **75**, 871.
39 R. S. S. Kumar, S. V. Rao, L. Giribabu and D. N. Rao, *Chem. Phys. Lett.*, 2007, **447**, 274–278.
40 N. Venkatram, D. N. Rao, L. Giribabu and S. V. Rao, *Appl. Phys. B: Lasers Opt.*, 2008, **91**, 149–156.
41 H. Bertagnolli, W. J. Blau, Y. Chen, D. Dini, M. P. Feth, S. M. O'Flaherty, M. Hanack and V. Krishnan, *J. Mater. Chem.*, 2005, **15**, 683–689.
42 Y. Chen, S. M. O'Flaherty, M. Hanack, O. Ito and W. J. Blau, *Adv. Mater.*, 2003, **15**, 899–902.
43 D. Dini and M. Hanack, in *The Porphyrin Handbook: Physical Properties of Phthalocyanine-based Materials*, ed. K. M. Kadish, K. M. Smith and R. Guilard, Academic Press, USA, 2003, vol. 17, p. 22.
44 N. Nwaji and T. Nyokong, *J. Lumin.*, 2017, **192**, 1167–1179.